USGS
science for a changing world

Seismic Velocity Site Characterization of 10 Arizona Strong-Motion Recording Stations by Spectral Analysis of Surface Wave Dispersion

By Robert E. Kayen, Brad A. Carkin, and Skye C. Corbett

Open-File Report 2016–1208

U.S. Department of the Interior
U.S. Geological Survey

U.S. Department of the Interior
RYAN K. ZINKE, Secretary

U.S. Geological Survey
William H. Werkheiser, Director

U.S. Geological Survey, Reston, Virginia: 2017

Suggested citation:
Kayen, R.E., Carkin, B.A., and Corbett, S.C., 2017, Seismic velocity site characterization of 10 Arizona strong-motion recording stations by spectral analysis of surface wave dispersion: U.S. Geological Survey Open-File Report 2016–1208, 32 p., https://doi.org/10.3133/ofr20161208.

ISSN 2331-1258 (online)

Contents

Abstract 1
Introduction 1
Study Sites 1
Rayleigh Wave Dispersion 4
  Adjustments for Missing 1st Wrapped Phase 6
  Inversion of the V_S Profile 6
Results 8
References Cited 8
Appendix 1. Site Data 10

Figures

Figure 1. Surface wave test locations of 11 sites in central and southern Arizona. 2

Tables

Table 1. Sites investigated in this study. 3

Seismic Velocity Site Characterization of 10 Arizona Strong-Motion Recording Stations by Spectral Analysis of Surface Wave Dispersion

By Robert E. Kayen, Brad A. Carkin, and Skye C. Corbett

Abstract

Vertical one-dimensional shear wave velocity (V_S) profiles are presented for strong-motion sites in Arizona for a suite of stations surrounding the Palo Verde Nuclear Generating Station. The purpose of the study is to determine the detailed site velocity profile, the average velocity in the upper 30 meters of the profile (V_{S30}), the average velocity for the entire profile (V_{SZ}), and the National Earthquake Hazards Reduction Program (NEHRP) site classification. The V_S profiles are estimated using a non-invasive continuous-sine-wave method for gathering the dispersion characteristics of surface waves. Shear wave velocity profiles were inverted from the averaged dispersion curves using three independent methods for comparison, and the root-mean-square combined coefficient of variation (*COV*) of the dispersion and inversion calculations are estimated for each site.

Introduction

This project focuses on the measurement of shear wave velocity (V_S) of the near-surface materials at strong-motion recording stations in Arizona. During two data collection campaigns, data were collected at 10 stations with recordings from prior earthquakes. These stations were regionally instrumented with permanent seismometer recording stations, some now moved or abandoned. The V_S profiles presented in this report are collected for input to ground motion prediction equations that factor in the effects of site amplification. Data presented here were gathered using the continuous harmonic sine wave approach for the spectral analysis of surface waves presented by Kayen and others (2004, 2013), which is a stepped sine wave method that utilizes a notch-filter methodology that improves on the approach of Satoh and others (1991). Continuous sine wave-source spectral analysis of surface waves (CSS–SASW) is an inexpensive and efficient means of non-invasively estimating the near-surface V_S of the ground. Though it is possible to measure V_S in cased boreholes or during penetration tests, these approaches tend not to be useful because they cannot reach the meaningful depths required for seismic site response analysis without expensive drilling and casing. Because many of the Arizona sites are stiff soil profiles or located on weathered bedrock, penetration methods are not useful.

Study Sites

The shear wave velocity profiles presented here are for strong-motion seismometer stations whose records are identified in the database of the Pacific Earthquake Engineering Research (PEER) Center and the Southwestern U.S. Ground Motion Characterization (SWUS-GMC) by the Senior Seismic Hazard Analysis Committee (SSHAC) Level 3 Project. The sites surround the Palo Verde Nuclear Generating Station (PVNGS) in central Arizona (fig. 1) out to approximately 100 miles.

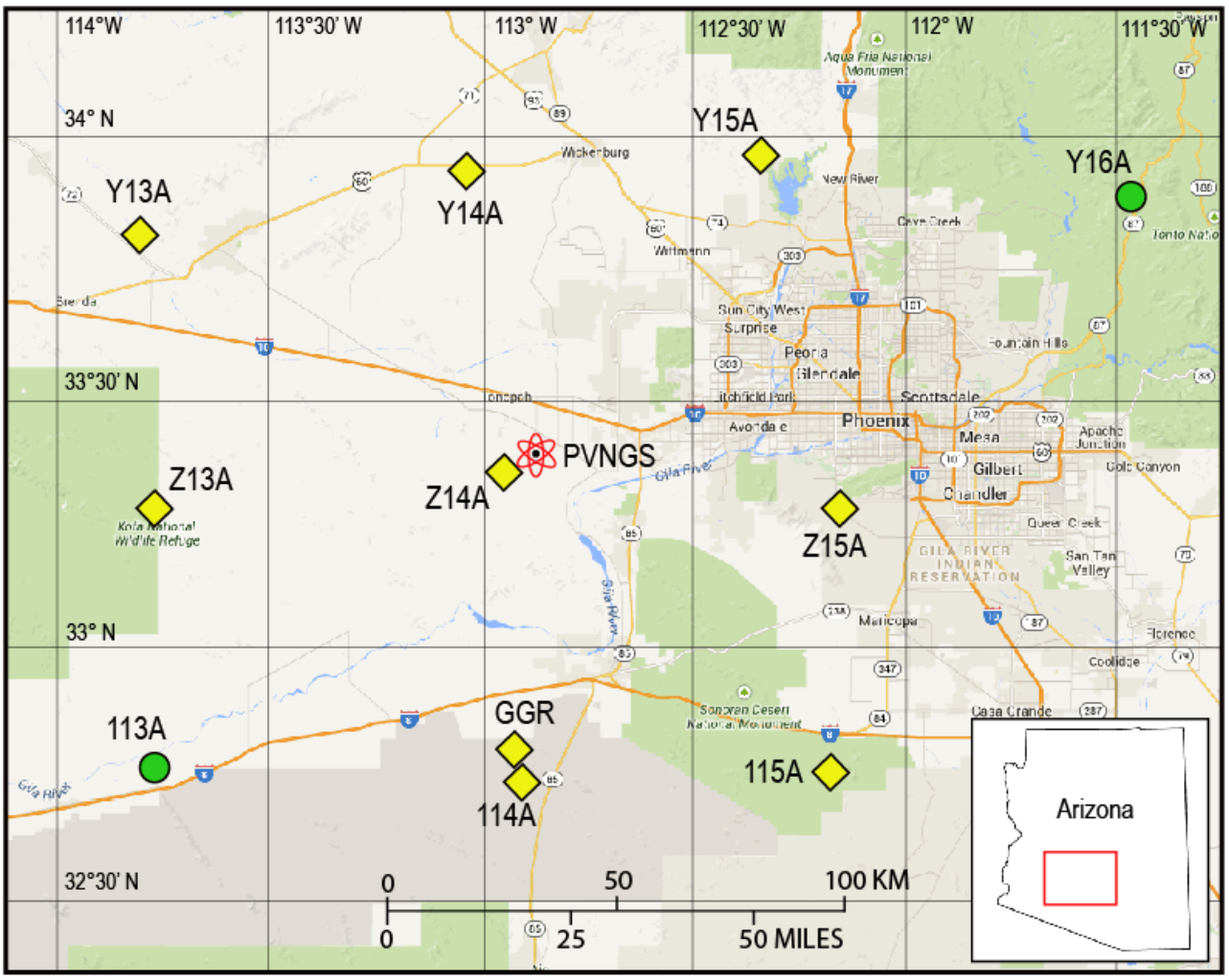

Figure 1. Surface wave test locations of 11 sites in central and southern Arizona. Symbols indicate National Earthquake Hazards Reduction Program site classifications; green circles are NEHRP site classification B sites and yellow diamonds are NEHRP site classification C sites. Red atom symbol is the Palo Verde Nuclear Generating Station (PVNGS) (base map from Google Maps).

Table 1. Sites investigated in this study.

[The table includes the Pacific Earthquake Engineering Research Center site ID, U.S. Geological Survey (USGS) test number, National Earthquake Hazards Reduction Program (NEHRP) site class, latitude, longitude, 30-meter average shear wave velocity V_{S30} from the automated inversion, V_{S30} from the manual inversion, V_{S30} from the Occam inversion, the maximum depth in meters (m) of the inversion, the average shear wave velocity for the entire profile to depth z, V_{SZ} from the automated inversion, the average V_{SZ} for the manual inversion, the average V_{SZ} for the Occam inversion, the average coefficient of variation (*COV*) of the group dispersion profile, the average coefficient of variation of the inversion, and the combined coefficient of variation. All velocities are in meters per second (m/s)]

Site ID	Z14A	115A	GGR	Y16A	Y15A	Z15A	113A	Y14A	Y13A-2	114A	Z13A
USGS test number	994	995	996	997	998	999	1000AZ	1001AZ	1002AZ	1003AZ	1004AZ
NEHRP CLASS	C	C	C	B	C	C	B	C	C	C	C
Latitude (°)	33.36094	32.70885	32.82366	33.87971	33.9527	33.2888	32.76984	33.93792	33.8176	32.75137	33.2006
Longitude (°)	−112.9449	−112.23207	−112.91518	−111.47787	−112.3343	−112.15735	−113.76493	−113.00282	−13.82913	−112.88342	−113.6506
V_{S30} (m/s) automated inversion	523.9	459.6	572.9	1028.3	565.5	406.6	1237.4	520.4	559.9	398.3	689.4
V_{S30} (m/s) manual inversion	508.1	443.0	599.5	988.1	545.1	464.3	1231.7	525.5	558.7	403.9	669.7
V_{S30} (m/s) Occam inversion	490	424	713.9	970	499	373	1140	473	532	380	652
MAX inversion depth (m)	107.7	99.1	54	40.2	40.2	39.4	38.3	49.9	50.2	50	50.1
V_{SZ} (m/s) automated inversion	522.0	528.0	788.8	1101.9	582.8	434.2	1598.5	575.7	610.6	423.9	777.7
V_{SZ} (m/s) manual inversion	688.6	541.0	830.9	1070.7	569.6	431.0	1385.1	586.1	607.7	445.1	763.0
V_{SZ} (m/s) Occam inversion	749	473	752.5	1023	476	437	1140	572	640	438	740
Dispersion average *COV*	0.0353	0.027	0.027	0.072	0.041	0.035	0.106	0.074	0.033	0.059	0.043
Inversion average *COV*	0.025	0.019	0.124	0.109	0.088	0.042	0.2	0.021	0.021	0.024	0.019
Combined *COV*	0.043	0.033	0.127	0.131	0.097	0.055	0.226	0.077	0.039	0.064	0.047

Rayleigh Wave Dispersion

Active-source surface wave analysis testing typically profiles the upper tens of meters of the ground using drop weights or harmonic sources. The upper 30 meters (m) are needed to compute the widely used site parameter V_{S30}, defined as 30 m divided by the shear wave travel time to a depth of 30 m. The CSS-SASW method employed in this study by the U.S. Geological Survey (USGS) is a technique that uses a parallel array of mass shakers. This method allows for profiling as deep as 100 m without the use of massive drop weights or heavy track-mounted machinery. For this method, we substitute an array of many low-frequency (1–100 hertz [Hz]) electromechanical shakers. Surface waves are generated with an array of two to eight APS Dynamics Model 400 shakers and amplifier units, powered by a generator and controlled by a spectral analyzer.

The shakers have a long stroke capable of cycling to as low as 1 Hz. The output signal from the spectral analyzer is split into a parallel circuit and sent to the separate amplifiers. The amplifiers power the shakers to produce a continuously vibrating, coherent, in-phase harmonic wave that vertically loads the ground. Most of this energy produces Rayleigh retrograde elliptical surface waves that propagate away from the source in a vertical, cylindrical wavefront perpendicular to the ground surface. The amplitude of the surface waves decay exponentially with depth, such that the energy of the wavefront is centered at a depth of approximately one-third to one-half the wavelength.

Frequency-domain analyses are made on two or more signals received by sensors placed in the field in the linear array some distance from the source. First, all channels of time-domain data are transformed into their equivalent linear spectrum in the frequency domain using a Fourier transform. One of the sensor's signals (typically the sensor closest to the source) is used for a reference input signal, and the other sensor signals are used to compute the linear spectra of the output. The separation distance from the reference seismometer to each output seismometer (d_s–d_{ref}) is later used to compute the wave velocity. The cross power spectrum $G_{xy}(\omega)$ is determined by multiplying the complex conjugate of the linear spectrum of the input signal $S_x^*(\omega)$ and the real portion of the linear spectrum of the output signal $S_y(\omega)$. The cross power spectrum is defined as

$$G_{xy}(\omega) = S_x^*(\omega) \times S_y(\omega) \quad (1)$$

The autopower spectrum, a measure of the energy at each frequency of the sweep, can be used to determine the strength of individual frequencies and is equal to the linear spectrum of a given sensor times its complex conjugate pair:

$$G_{xx}(\omega) = S_x(\omega) \times S_x^*(\omega) \quad (2)$$

$$G_{yy}(\omega) = S_y(\omega) \times S_y^*(\omega) \quad (3)$$

A cross power spectrum can be represented by its real and imaginary components for its phase, θ, and magnitude, m. The phase is the relative lag between the signals at each frequency, and the magnitude is a measure of the power between the two signals at each frequency. Because the phases are relative, they can be stacked to enhance signal-to-noise ratio of the phase lag at each frequency.

The phase of the cross power spectrum is computed as the inverse tangent of the ratio of the imaginary and real portions of the cross power spectrum:

$$\theta_{xy}(\omega) = \tan^{-1}\frac{Im(G_{xy}(\omega))}{Re(G_{xy}(\omega))} \quad (4)$$

The travel time $t(f)$ of one cycle of a wave of frequency (f) is computed as

$$t(f) = \theta(\omega)/\omega \tag{5}$$

and the wavelength, λ, at each frequency is

$$\lambda(\theta) = (d_s – d_{ref})/\ \theta(f) \tag{6}$$

The Rayleigh wave velocity, V_R, is computed as

$$\begin{aligned} V_r(f) &= (d_s – d_{ref})/t(f) \\ &= f(d_s – d_{ref})\ 360°/\theta \text{ (degrees)} \\ &= f(d_s – d_{ref})\ 2\pi/\theta(\phi) \text{ (radians)} \\ &= f\lambda\ (f) \end{aligned} \tag{7}$$

The SASW procedure maps the change in θ across the frequency spectrum and merges these phase lags with the sensor array geometry to measure velocity. Typically, with the shaker source, the discrete frequencies are cycled in a swept-sine (stepped) fashion across a range of low frequencies (1–200 Hz). Rayleigh wave phase velocity is then mapped in frequency or wavelength space. This velocity map or profile is called a dispersion curve and characterizes changes in the frequency-dependent Rayleigh wave velocity. The evaluation of velocities is constrained to the wavelength zone where $\lambda(f)/3 < (d_s – d_{ref}) < 2\lambda(f)$ for typical data and $\lambda(f)/3 < (d_s – d_{ref}) < 3\lambda(f)$ for excellent data, corresponding to phase lags of 180°–1,080° (typical data) and 120°–1,080° (excellent data). At longer and shorter wavelengths, the data become unreliable for computing velocities.

Because the useable wavelengths are constrained by the seismometer separation, the array is expanded to capture Rayleigh wave dispersion representative of a specific range of wavelengths. The near surface is characterized by short wavelengths and high frequencies, whereas the deeper portion of the profile is characterized by long wavelengths and low frequencies. Each wavelength range requires a separate independent test that is merged together with other wavelength ranges to determine an average dispersion curve for the site.

At the largest seismometer separations, the increasing area of the wavefront causes the wave amplitude to diminish, owing to geometric damping, and the overall quality of the data diminishes. Two measures of data quality are used to evaluate the field measurements in the frequency domain. Coherence, $\gamma^2(\omega)$, is a normalized real function with values between 0 and 1, corresponding to the ratio of the power of the cross power spectrum, $G_{yx}(\omega)\bullet G_{yx}^*(\omega)$, to the autopower spectrum of the outboard seismometer, $G_{xx}(\omega)\bullet G_{yy}(\omega)$. Values close to 1 indicate high correlation between the reference and outboard seismometers across narrow frequency bands. This is a useful data quality parameter for hammer impact data.

$$\gamma_{xy}^2(\omega) = \frac{G_{yx}(\omega)\bullet G_{yx}^*(\omega)}{G_{xx}(\omega)\bullet G_{yy}(\omega)} \tag{8}$$

For swept-sine data where discrete frequencies are used to compute phase rather than narrow frequency bands, the frequency response function (FRF) is a complex measure of the data quality of the output (outboard) seismometer and is sometimes called the transfer function:

$$\mathrm{FRF}(\omega) = \frac{G_{yx}(\omega)}{G_{xx}(\omega)} \tag{9}$$

where x is the input (reference) signal and y is the response (output) signal.

The frequency response function is a two-sided complex parameter. To convert to the frequency response gain (magnitude) that is used to evaluate the amplitude of the output response to the input stimulus, a rectangular-to-polar coordinate conversion is used.

Adjustments for Missing 1st Wrapped Phase

At some sensor separations, the field data have a poorly formed first phase such that the first clear wrapped-phase crossing occurs not at 180° but at 540°. For these dispersion data files, a simple reprocessing was done to add one phase jump (360°, 2π) to the dispersion curves preceding the 540° jump to adjust the file to the correct wrapped-phase number. This adjustment corrects the wavelength calculation as follows:

$$\lambda_{(corrected)} = 2\pi((d_s - d_{ref})\ (\theta + 2\pi) \tag{10}$$

With the wavelength adjusted, the velocity, V_R, decreases by

$$V_R = f \bullet 2\pi((d_s - d_{ref})/(\theta + 2\pi) \tag{11}$$

The effect of correcting the phase wrap and reducing the calculated wavelength is to reduce the depth of influence of the adjusted dispersion curve.

Inversion of the V_S Profile

The relation between Rayleigh wave (V_R), shear wave (V_S) and compression wave () velocities can be formulated through Navier's equations for dynamic equilibrium. On the surface of the ground, and in the case of plane strain, the following characteristic equation can be applied:

$$\frac{V_R}{V_s}^6 - 8\ \frac{V_R}{V_s}^4 + \left[24 - 16\left[\frac{1-2\nu}{2(1-\nu)}\right]\right]\frac{V_R}{V_s}^2 + 16\left[\left[\frac{1-2\nu}{2(1-\nu)}\right] - 1\right] = 0 \tag{12}$$

where ν is the Poisson ratio and

$$\frac{V_S}{V_P} = \gamma = \sqrt{\left[\frac{1-2\nu}{2(1-\nu)}\right]} \tag{13}$$

For reasonable values of Poisson ratio for earth materials, between 0.30 and 0.49, Viktorov (1967) shows that the shear wave velocity ranges between 105 and 115 percent of the measured Rayleigh wave velocity.

$$\frac{V_R}{V_S} = K = \frac{0.87+1.12\nu}{1+\nu} \tag{14}$$

such that across the range $0.2 < \nu < 0.49$, the range of K is $0.87 < K < 0.96$.

The inversion method seeks to infer an acceptable best-fit model of seismic shear wave velocity, V_S, of the ground given the measured dispersive characteristics of Rayleigh waves observed in the frequency domain and the estimated profile of Poisson ratio and material density. The inversion attempts to build a model from observations, as opposed to the normal prediction of behavior based upon a model. If the inversion model is simple and linear, it will result in a unique and stable solution. The French mathematician Hadamard defined mathematical problems that have solutions that exist, are unique, and are stable as “well-posed” (Zhdanov, 2002). On the other hand, surface wave inversion is an

"ill-posed" inverse problem, as solutions are not unique, the solutions may become unstable, and multiple shear wave velocity profiles can result in approximately the same dispersion curve (Zhdanov, 2002).

The dispersive characteristic of Rayleigh wave propagation allows us to infer the V_S at depth based on measurements at the free surface. The inversion problem computes the Rayleigh wave phase velocity (V_R) from laterally constant layers of an infinite half space. For each of these layers, the shear modulus, Poisson ratio, density, and thickness are unknown. Displacements for a vertically acting harmonic point load can be computed as follows in the far field if we neglect body wave components:

$$u_\beta(r,z,\omega) = F_z \cdot G_\beta \cdot (r,z,\omega) \cdot e^{i[\omega t - \psi_\beta(r,z,\omega)]} \quad (15)$$

where β stands for the generic component either vertical or radial, $G_\beta(r,z,\omega)$ is the Rayleigh geometrical spreading function, and $\Psi_\beta(r,z,\omega)$ is the composite phase function (Lai and Rix, 1998).

Regularization methods have been developed for solving the ill-posed inversion problem: for example, the velocity profiles computed here. The Levenberg-Marquardt method, also called damped least squares, is one example of a regularization method. These and other techniques, such as artificial neural networks and genetic algorithms, are discussed by Santamarina and Fratta (1998). One cost of these stochastic methods is that they often require many more iterations, and so they are much more computationally intensive.

The parameters of the inversion problem can be chosen such that the difference between the observational dispersion data and the output of the inversion problem are minimized. Such a constraint is insufficient for ill-posed problems because many solutions can fit the data equally well and some of these solutions will be physically unrealistic. The most common approach is to constrain the inversion solution space by selecting the smoothest solution from a suite of solutions that all exhibit a sufficient goodness-of-fit to the observed data, as indicated by a root-mean-square (RMS) error minimum (Constable and others, 1987).

An empirical approach serves as a counterpoint to the inversion methods used in this report. Pelekis and Athanasopoulos (2011) advanced the work of Satoh and others (1991) in a technique termed the SIM (simplified inversion method), which computes the shear wave velocity profile as a function of the incremental slope of the Rayleigh wave dispersion curve, where D_n is the depth at layer n:

$$V_{Sn,normal\ dispersion} = 1.1 \cdot \frac{\bar{V}_{Rn}D_n - \bar{V}_{Rn-1}D_{n-1}}{D_n - D_{n-1}} \quad (16)$$

$$V_{Sn,inverted\ dispersion} = 1.1 \cdot \frac{D_n - D_{n-1}}{D_n/\bar{V}_{Rn} - D_{n-1}/\bar{V}_{Rn-1}} \quad (17$$

The dispersion curve, V_R, plotted against λ_R is converted into an apparent velocity ($\bar{V}_R$) and depth (z) by converting λ_R to an estimated depth of $z_{eq} = a_R \cdot \lambda_R \approx 0.635\lambda_R$. The parameter a_R is a penetration depth coefficient optimized to achieve a minimum weighted average difference between the simplified velocity profile and that computed through the more advanced inversion of Pelekis and Athanasopoulos (2011). The average apparent phase velocity, $\overline{V_R}$, is approximated as the velocity at each segment node (layer interface) of a multilinear curve fit to the dispersion curve. A positive slope of a segment indicates normal dispersion; a negative slope indicates inverted dispersion. The value of V_S for each individual layer is calculated using the equations 16 and 17 above for the cases of normal dispersion or inverted dispersion, respectively. The approach of Pelekis and Athanasopoulos (2011) improves on the Satoh and others (1991) method notably by optimizing the penetration depth coefficient a_R.

Results

We provide two profile solutions at each site: inversion and SIM. We varied the assumptions about the layer thicknesses and the threshold RMS error that determines if the inversion has converged to best characterize the site. The decision as to whether or not the more complex model is warranted by the fit of the theoretical dispersion curve (TDC) to the empirical dispersion curve (EDC) is subjective. Table 1 summarizes results and provides the SASW site ID, the site description, the date of data collection, the latitude and longitude of the SASW test site, and the V_{S30}.

Appendix 1 includes plots of the model profiles and the EDC and TDCs for each site. Appendix 1 also includes the site photos and a vicinity map for each site. Where possible we have indicated the location of the strong-motion station in the site photographs and vicinity maps to assess the distance between the SASW survey and the strong-motion station. NEHRP classification is used to average the site conditions in the upper-30 meters of ground (V_{S30} from the International Code Council, 2002). Equation 18 is used to compute this average velocity based on the unit layer thickness (d_i) and the corresponding interval velocity (V_{Si}).

$$V_{Si-depth-averaged} = \frac{\sum_{i=1}^{n} d_i}{\sum_{i=1}^{n} \frac{d_i}{V_{Si}}} \tag{18}$$

These site categories are used to assign design spectra in the evaluation of performance for new and built structures.

A statistical analysis of the shear wave velocity of the upper 30 m was computed by determining the average coefficient of variation (COV_{DIS}) of the dispersion curve from the group phase velocity and the average coefficient of variation (COV_{INV}) of shear wave velocity profiles computed in the inversions that satisfied the minimum acceptable inversion model variance.

The mean values of the group dispersion curves were calculated by binning the dispersion curve values in terms of wavelength (for example, in 1-m bins) or frequency (for example, in 1-Hz bins) and then averaging the values within each bin. The coefficient of variation was calculated by dividing the binned standard deviation of the velocity values by the binned mean values. The mean and standard deviation of the shear wave velocity layers of the inversion were calculated by averaging the layer values for the suite of profiles that satisfy the lowest possible RMS error, separating the theoretical inversion-based and empirical field-dispersion curves.

For both the dispersion curve and the inversion-based coefficients of variation, the average coefficient of variation was determined for the profiles. The overall model coefficient of variation was computed as the RMS of the dispersion *COV* and the inversion *COV* (equation 19).

$$COV_{MODEL} = \sqrt{{COV_{DIS}}^2 + {COV_{INV}}^2} \tag{19}$$

For the deep, stiff soil sites, the combined dispersion and inversion *COV* was typically less than 0.07, reflecting the remarkably good dispersion data sets and the gentle monotonic increasing nature of the velocity profiles. For sites situated on rock, the combined *COV* ranges from 0.12 to 0.23, reflecting greater variance in the field dispersion data and the inverted profiles.

References Cited

Constable, S.C., Parker, R.L., and Constable, G.G., 1987, Occam's Inversion—A practical algorithm for generating smooth models from electromagnetic sounding data: Geophysics, v. 52, no.3, p. 289–300.

International Code Council, 2002, International Building Code: Falls Church, Va., International Code Council, 756 p.
Kayen, R., Seed, R.B., Moss, R.E., Cetin, O., Tanaka, Y., and Tokimatsu, K., 2004, Global shear wave velocity database for probabilistic assessment of the initiation of seismic soil liquefaction: Proceedings of the 11th International Conference on Soil Dynamics and Earthquake Engineering, Berkeley, Calif., v. 2, p. 506–512.
Kayen, R., Moss, R., Thompson, E., Seed, R., Cetin, K., Kiureghian, A., Tanaka, Y., and Tokimatsu, K., 2013, Shear-wave velocity–based probabilistic and deterministic assessment of seismic soil liquefaction potential: Journal of Geotechnical and Geoenvironmental Engineering, v. 139, no. 3, p. 407–419. [Also available at http://dx.doi.org/10.1061/(ASCE)GT.1943-5606.0000743.]
Lai, C.G., and Rix, G.J., 1998, Simultaneous inversion of Rayleigh phase velocity and attenuation for near-surface site characterization, Georgia Institute of Technology, School of Civil and Environmental Engineering, Report No. GIT-CEE/GEO-98-2, 258 p.
Pelekis, P.C., Athanasopoulos, G.A., 2011, An overview of surface wave methods and a reliability study of a simplified inversion technique, Soil Dynamics and Earthquake Engineering, v. 32, no. 12, p. 1654–1668, doi:10.1016/j.soildyn.2011.06.012.
Santamarina, J.C., and Fratta, D., 1998, Introduction to discrete signals and inverse problems in civil engineering: Reston, Va., American Society of Civil Engineers Press, 327 p.
Satoh, T., Poran, C.I., Yamagata, K., Rondriquez, J.A., 1991, Soil profiling by spectral analysis of surface waves, *in* Proceedings of the Second International Conference On Recent Advances in Geotechnical Earthquake Engineering and Soil Dynamics, Vol. II, St. Louis, Mo., March 11–15, 1991: University of Missouri-Rolla, Paper No. 10.23, p.1429–1434.
Viktorov, I.A., 1967, Rayleigh and Lamb waves—physical theory and applications: New York, Plenum Press, 154 p.
Zhdanov, M.S., 2002, Geophysical Inverse Theory and Regularization Problems; Methods in Geochemistry and Geophysics, 36: Amsterdam, Elsevier, 628 p.

Appendix 1. Site Data

The following pages present the individual site location photographs, location map, field and computed velocity data, dispersion curves, and inversion profiles. Shear wave velocity values for 30 meters and the maximum profile depth are presented for the three inversion methods as well as the coefficient of variation of these parameters.

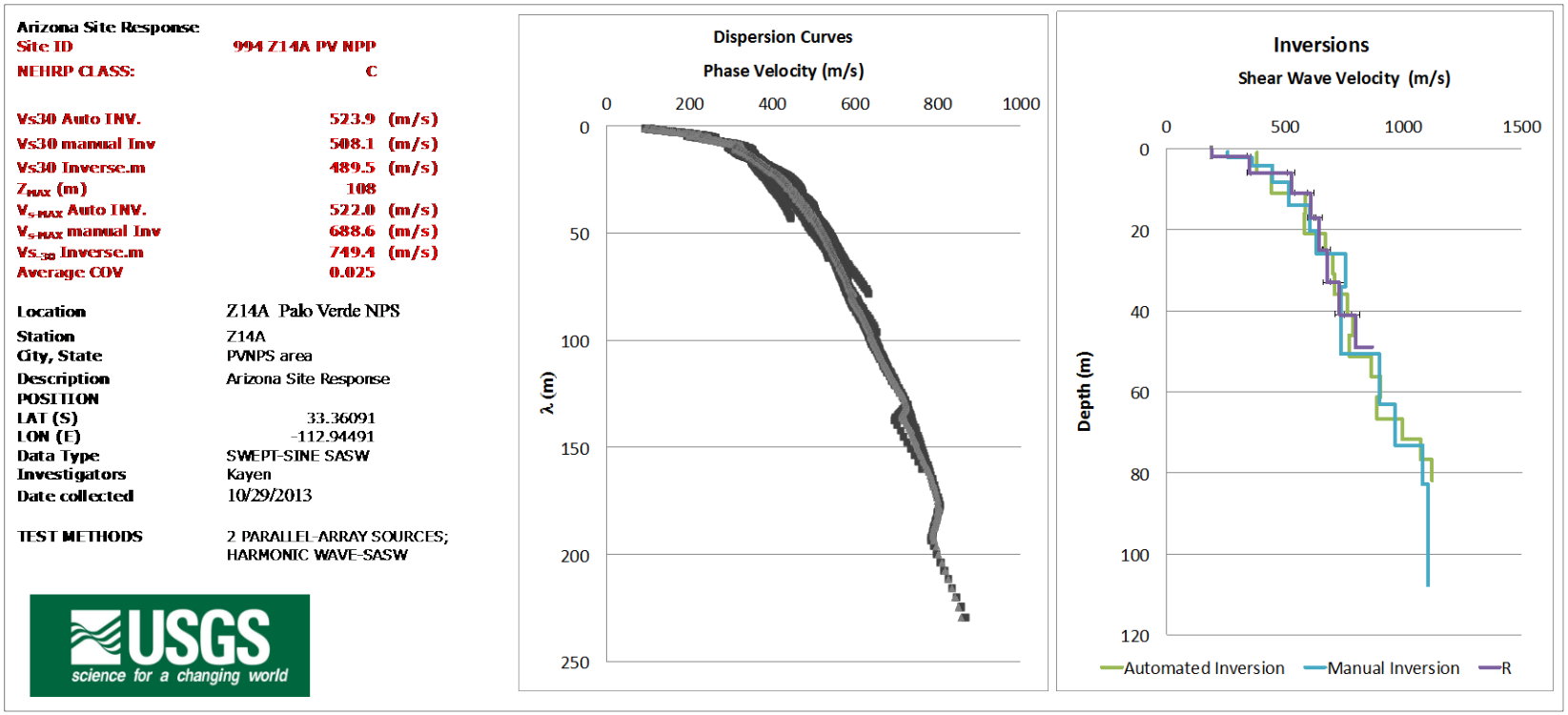

Figure 1. Site ID, location, and average shear wave velocity (left) for surface wave test site 994-Z14A; average dispersion curve in gray, and individual empirical dispersion curves in black (center plot); shear wave velocity profile computed by three inversion methods (right plot).

Figure 2. Surface wave test site 994–Z14A located (lat 33.36094, long –112.9449) on South 415th Avenue, Tonopah, Arizona, 8 kilometers southwest of the Palo Verde Nuclear Generating Station, Arizona. The test site is located about 200 meters south-southeast of the USArray seismometer location (33.36275 –112.94577). *A*, view towards the west from the shaker trailer; *B*, another view to the west along the seismometer array; *C*, view to the east to the shaker trailer; *D*, another view to the east; *E*, satellite view of the local site, yellow bar is seismometer array; *F*, the site location in Arizona.

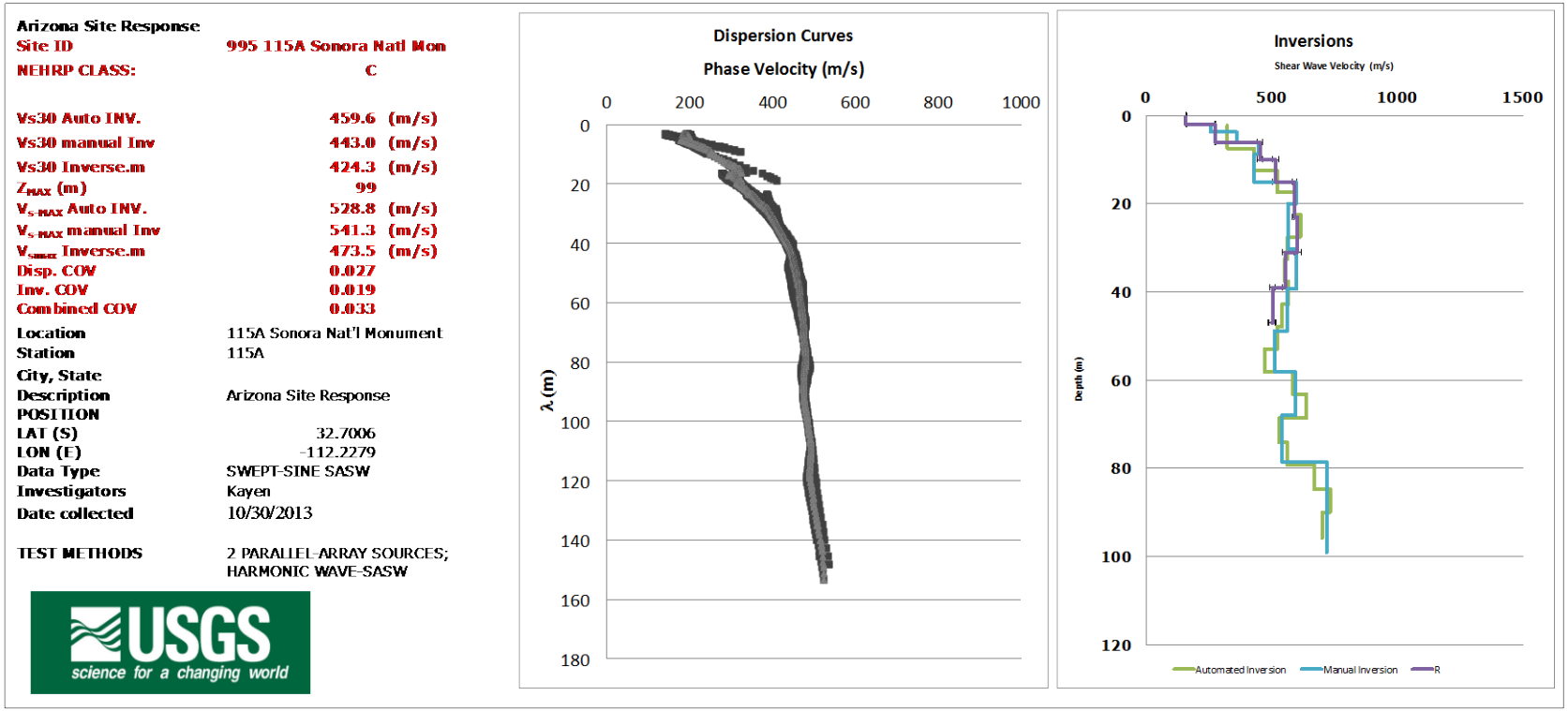

Figure 3. Site ID, location, and average shear wave velocity (left) for surface wave test site 995-115A; average dispersion curve in gray, and individual empirical dispersion curves in black (center plot); shear wave velocity profile computed by three inversion methods (right plot).

Figure 4. Surface wave test site 995-115A located (lat 32.70885, long –112.23207) adjacent to Vekol Valley Road in the Sonoran Desert National Monument, 15 kilometers south of Interstate 8, Arizona. The test site is about 1 kilometers north-northwest of the location of the USArray seismometer (lat 32.7006, long –112.2279). *A*, view looking eastward to the shaker trailer; *B*, view westward along the seismometer array; *C*, another view eastward to the shaker trailer; *D*, sign on Vekol Valley Road near Interstate 8; *E*, satellite view of the local site, yellow bar is seismometer array; F, site location in Arizona.

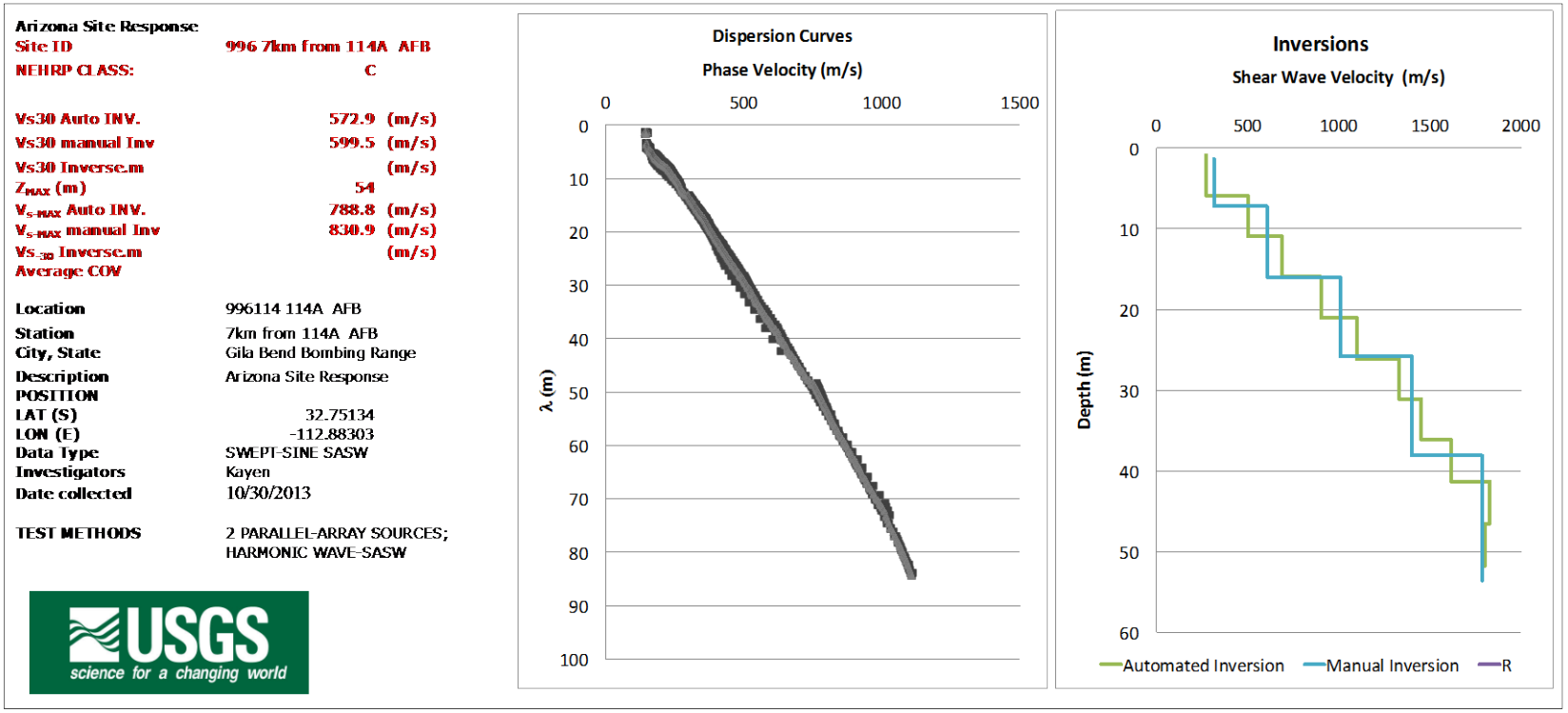

Figure 5. Site ID, location, and average shear wave velocity (left) for surface wave test site 996-GGR; average dispersion curve in gray, and individual empirical dispersion curves in black (center plot); shear wave velocity profile computed by three inversion methods (right plot).

Figure 6. Surface wave test site 996-GGR (Goldwater Gunnery Range) located (lat 32.82366, long –112.91518) on the U.S. Air Force Barry M. Goldwater Gunnery Range, Arizona. The test site is located 8.7 kilometers north-northwest of the USArray seismometer installation (lat 32.75134, long –112.88303). *A*, view northward to the shaker trailer, the seismometer array extends to the left; *B*, view to the southeast across the seismometer array; *C*, view southwest to the shaker trailer; *D*, another view to the southeast to the shaker trailer; *E*, satellite view of the local site, yellow bar is seismometer array; *F*, site location in Arizona.

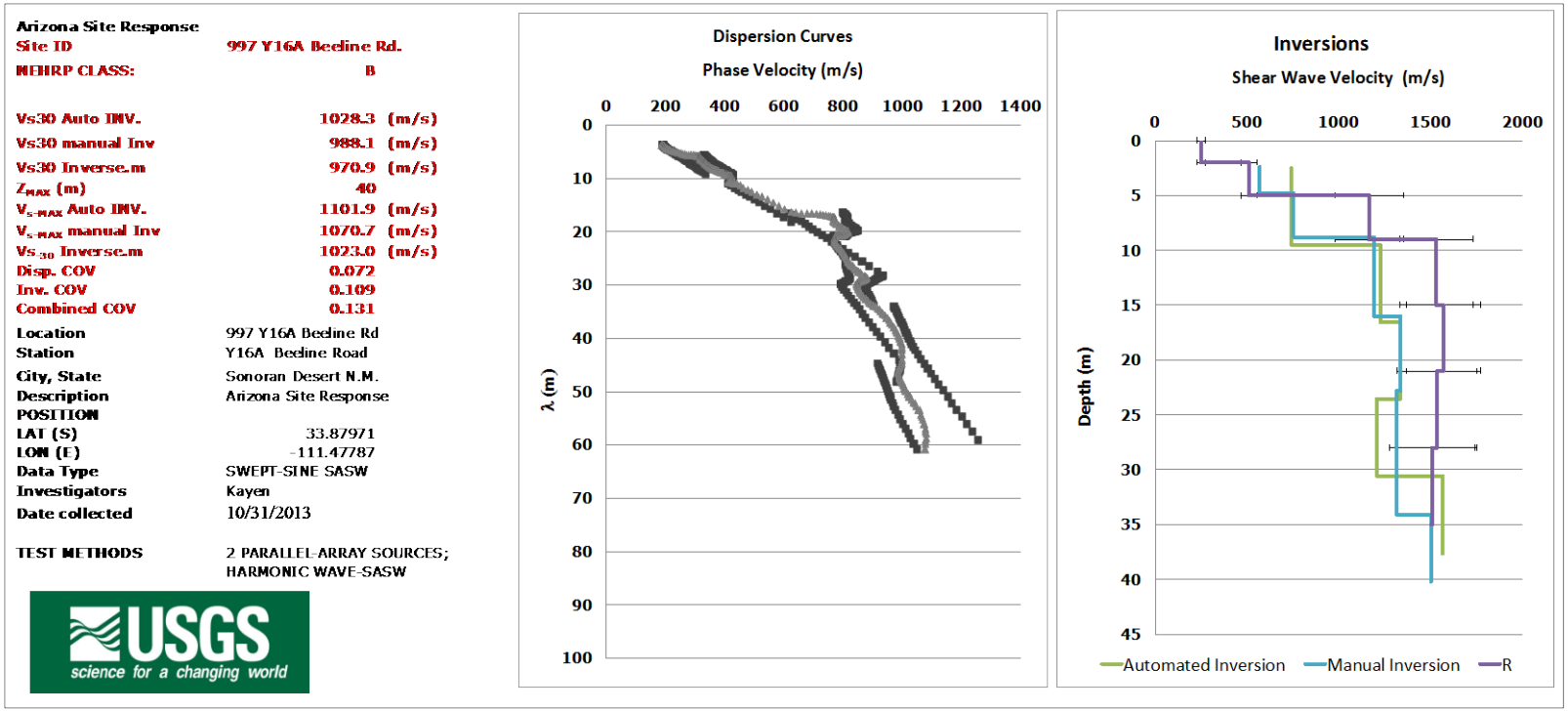

Figure 7. Site ID, location, and average shear wave velocity (left) for surface wave test site 997-Y16A; average dispersion curve in gray, and individual empirical dispersion curves in black (center plot); shear wave velocity profile computed by three inversion methods (right plot).

Figure 8. Surface wave test site 997-Y16A located (lat 33.87971, long –111.47787) near N. Beeline Highway, about 1.7 kilometers from Highway 87 and about 70 kilometers northeast of Phoenix, Arizona. *A*, view to the west to the shaker trailer; *B*, view to the east to the shaker trailer; *C*, view west along the seismometer array; *D*, view to the east from the shaker trailer; *E*, satellite view of the local site, yellow bar is seismometer array, the yellow star is the USArray seismometer location, Beeline Highway is at the upper right; *F*, site location in Arizona.

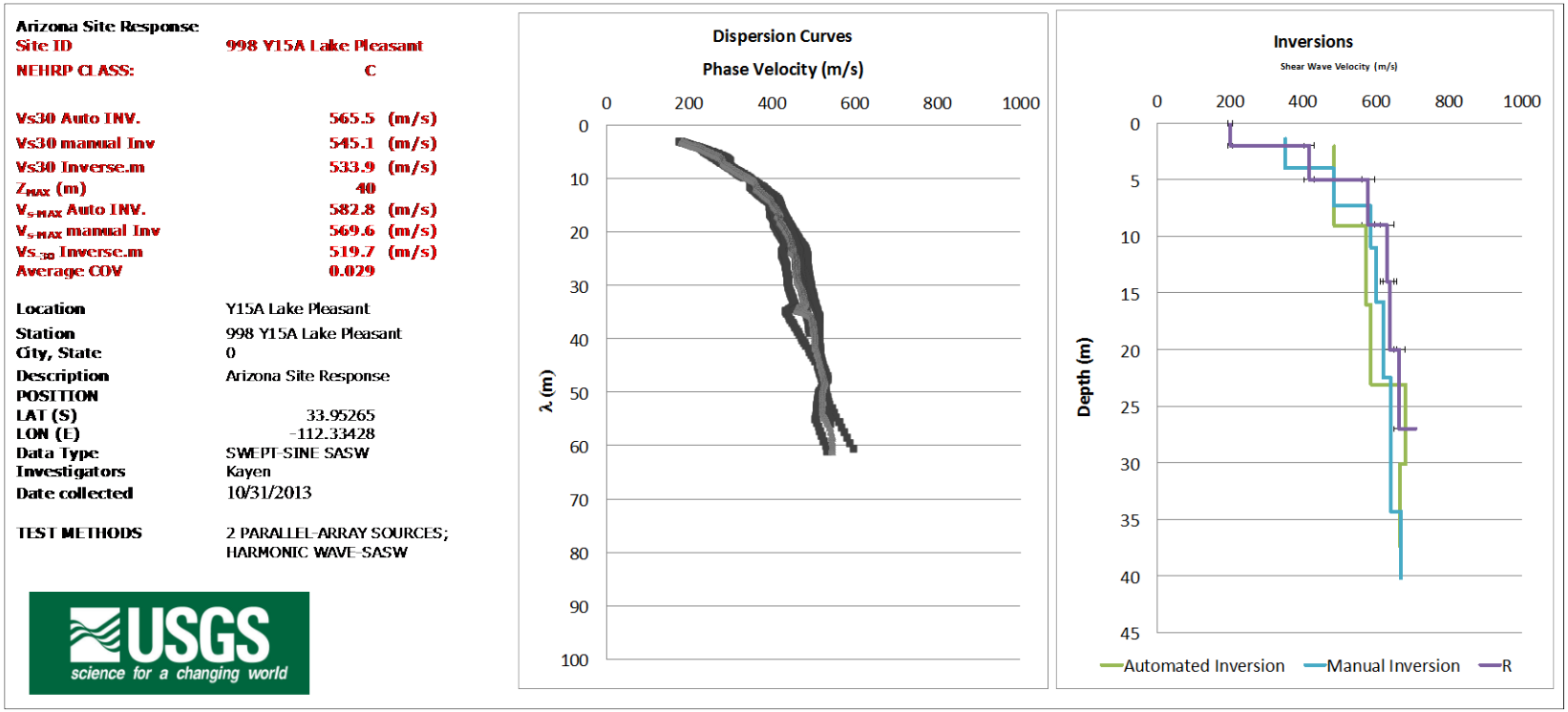

Figure 9. Site ID, location, and average shear wave velocity (left) for surface wave test site 998-Y15A; average dispersion curve in gray, and individual empirical dispersion curves in black (center plot); shear wave velocity profile computed by three inversion methods (right plot).

Figure 10. Surface wave test site 998-Y15A located (lat 33.95265, long –112.33428 W) on N. Castle Hot Springs Road, northwest of Lake Pleasant, Arizona. *A*, view to the southwest to the shaker trailer; *B*, another view to the southwest along the seismometer array; *C*, view northeast on the seismometer array; *D*, USArray seismometer; *E*, satellite view of the local site, yellow bar is seismometer array, the yellow star is the USArray seismometer location; *F*, site location in Arizona.

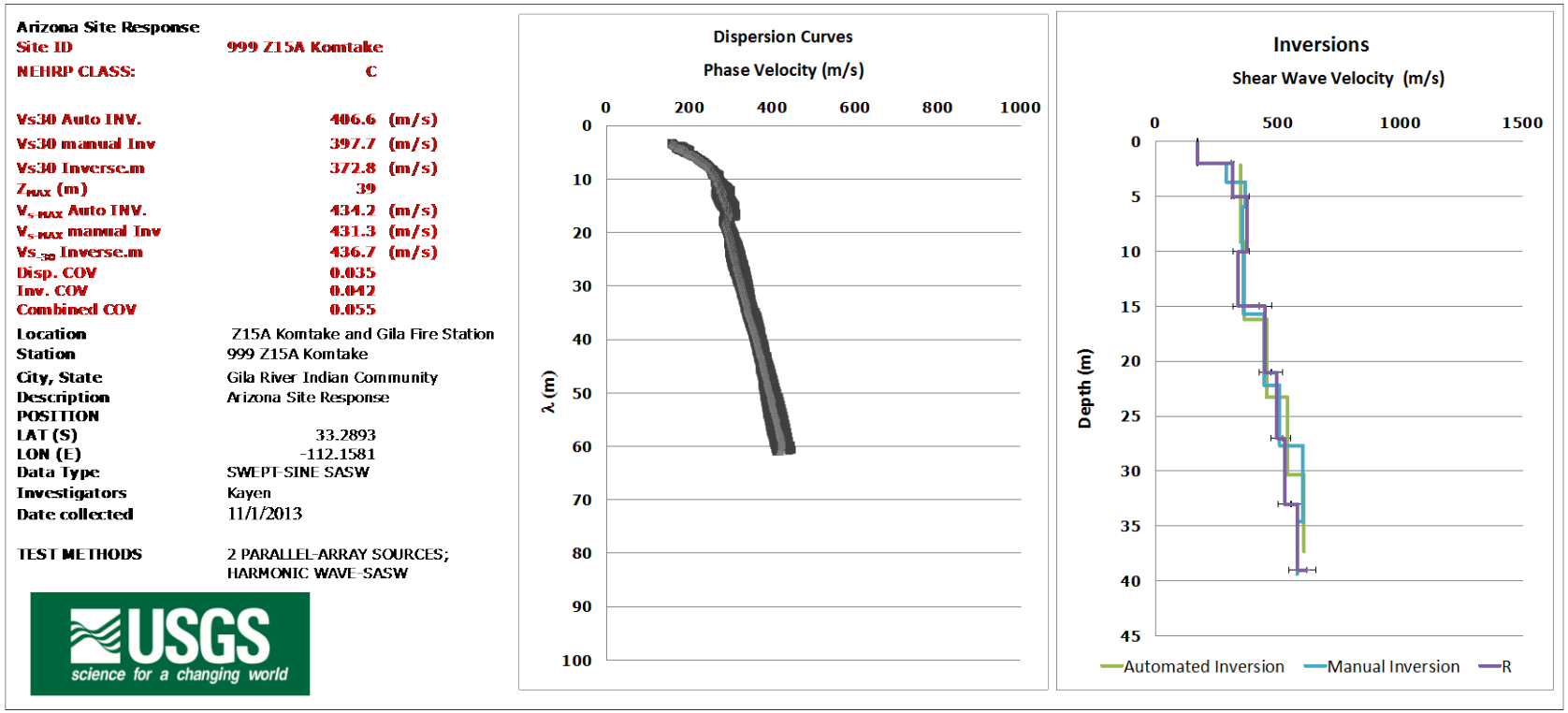

Figure 11. Site ID, location, and average shear wave velocity (left) for surface wave test site 999-Z15A; average dispersion curve in gray, and individual empirical dispersion curves in black (center plot); shear wave velocity profile computed by three inversion methods (right plot).

Figure 12. Surface wave test site 999-Z15A located (lat 33.2888, long –112.15735) in District 6 (Komatke), Gila River Indian Community, Arizona. *A*, view looking westward to the seismometer array location (dashed yellow line); *B*, view west to the shaker trailer parked on S. Health Care Drive; *C*, view northeast to the shaker trailer; *D*, view southwest to the shaker trailer; *E*, satellite view of the local site, yellow bar is seismometer array, the yellow star is the location of the USArray seismometer; *F*, site location in Arizona.

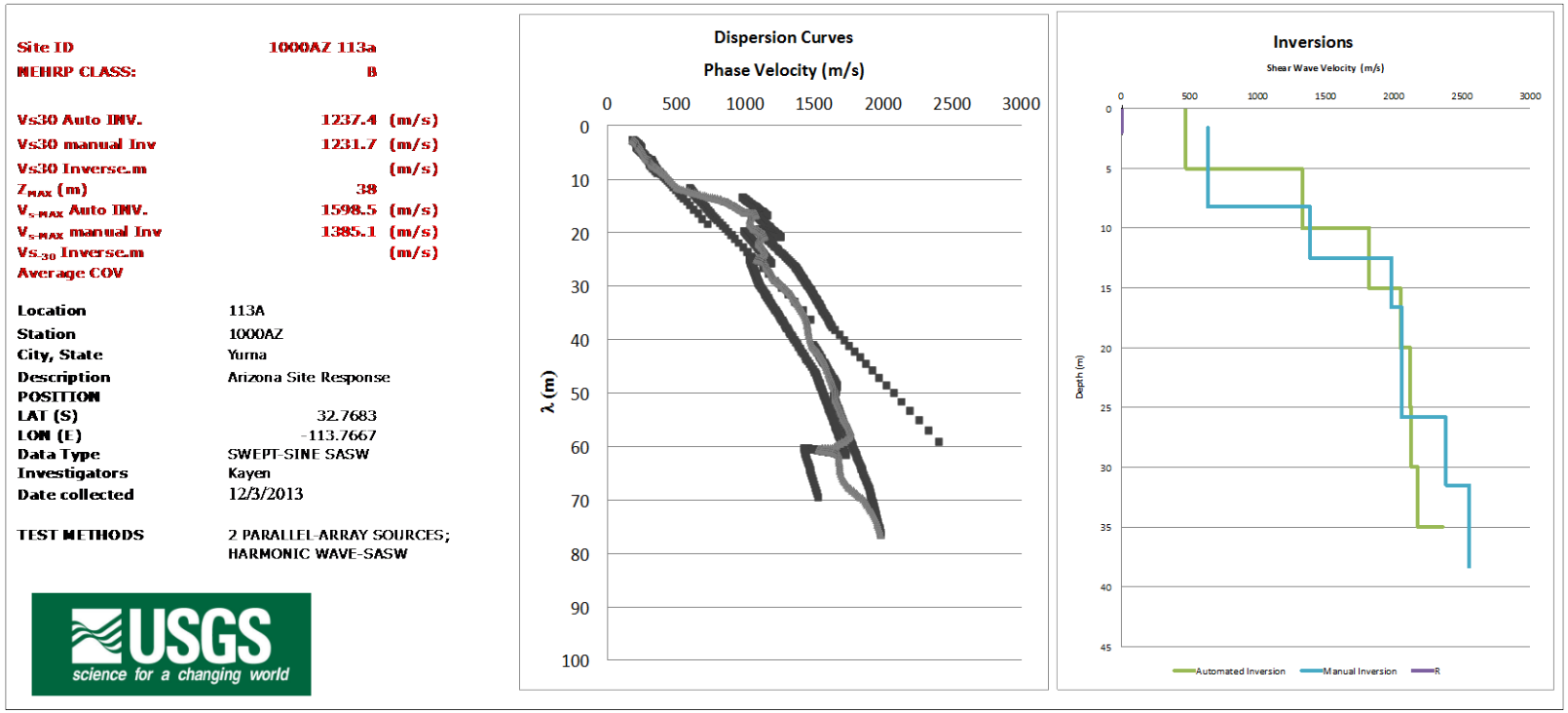

Figure 13. Site ID, location, and average shear wave velocity (left) for surface wave test site 1000AZ-113A; average dispersion curve in gray, and individual empirical dispersion curves in black (center plot); shear wave velocity profile computed by three inversion methods (right plot).

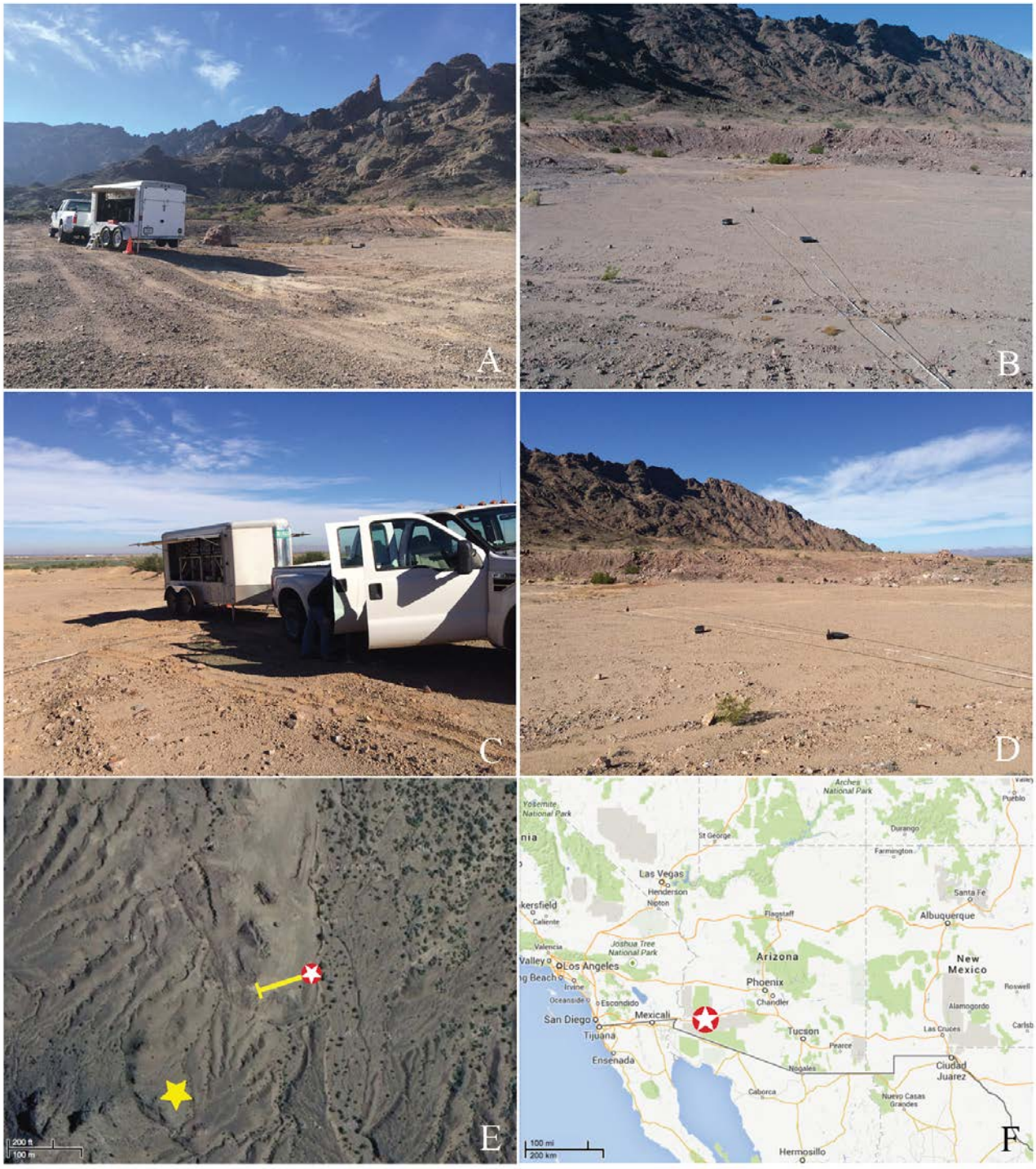

Figure 14. Surface wave test site 1000-113A located (lat 32.76984, long –113.76493) 76 kilometers east of Yuma, Arizona. *A*, view to the southwest to the shaker trailer; *B*, view westward to the seismometer array; *C*, view northeast to the shaker trailer; *D*, view northwest to the seismometer array; *E*, satellite view of the local site, yellow bar is seismometer array, the yellow star is the location of the USArray seismometer; *F*, site location in Arizona.

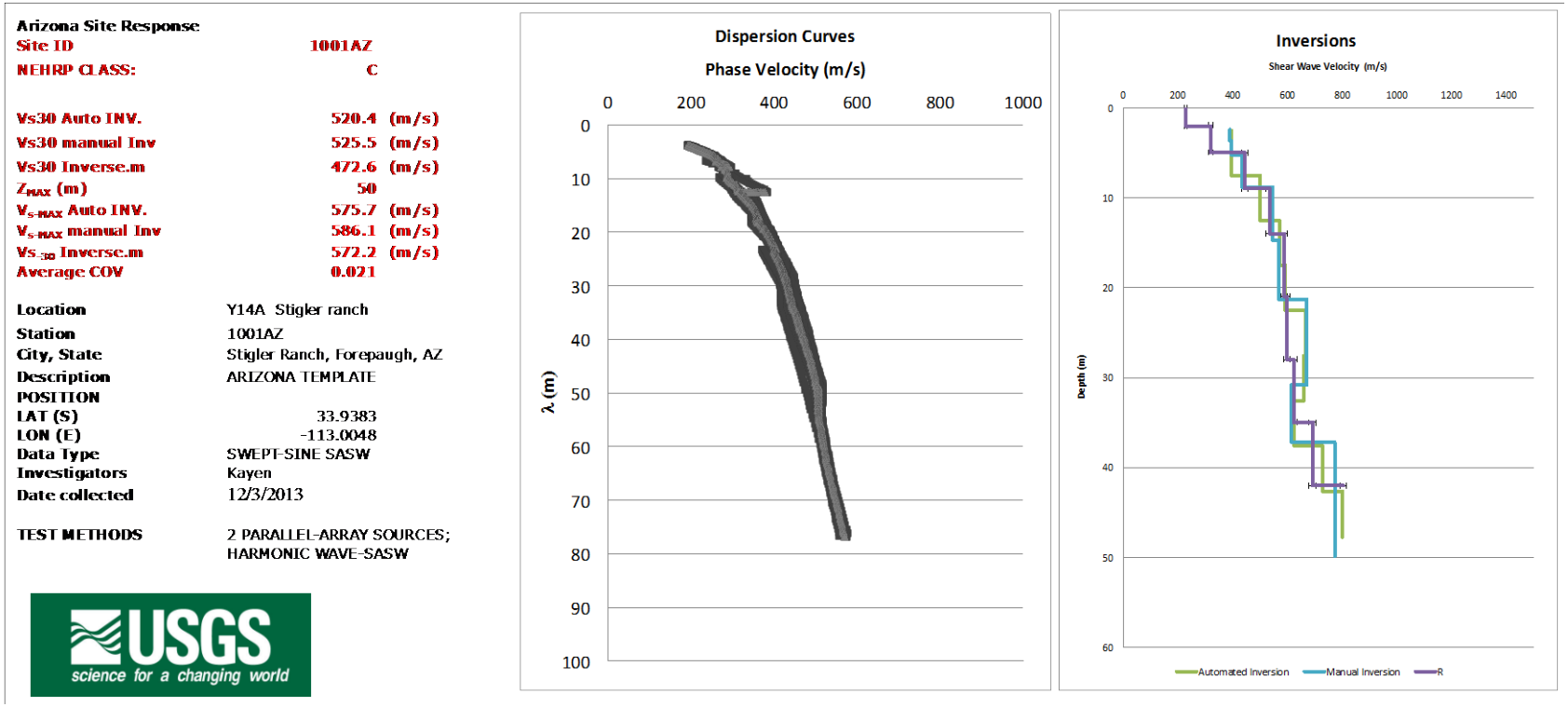

Figure 15. Site ID, location, and average shear wave velocity (left) for surface wave test site 1001AZ-Y14A; average dispersion curve in gray, and individual empirical dispersion curves in black (center plot); shear wave velocity profile computed by three inversion methods (right plot).

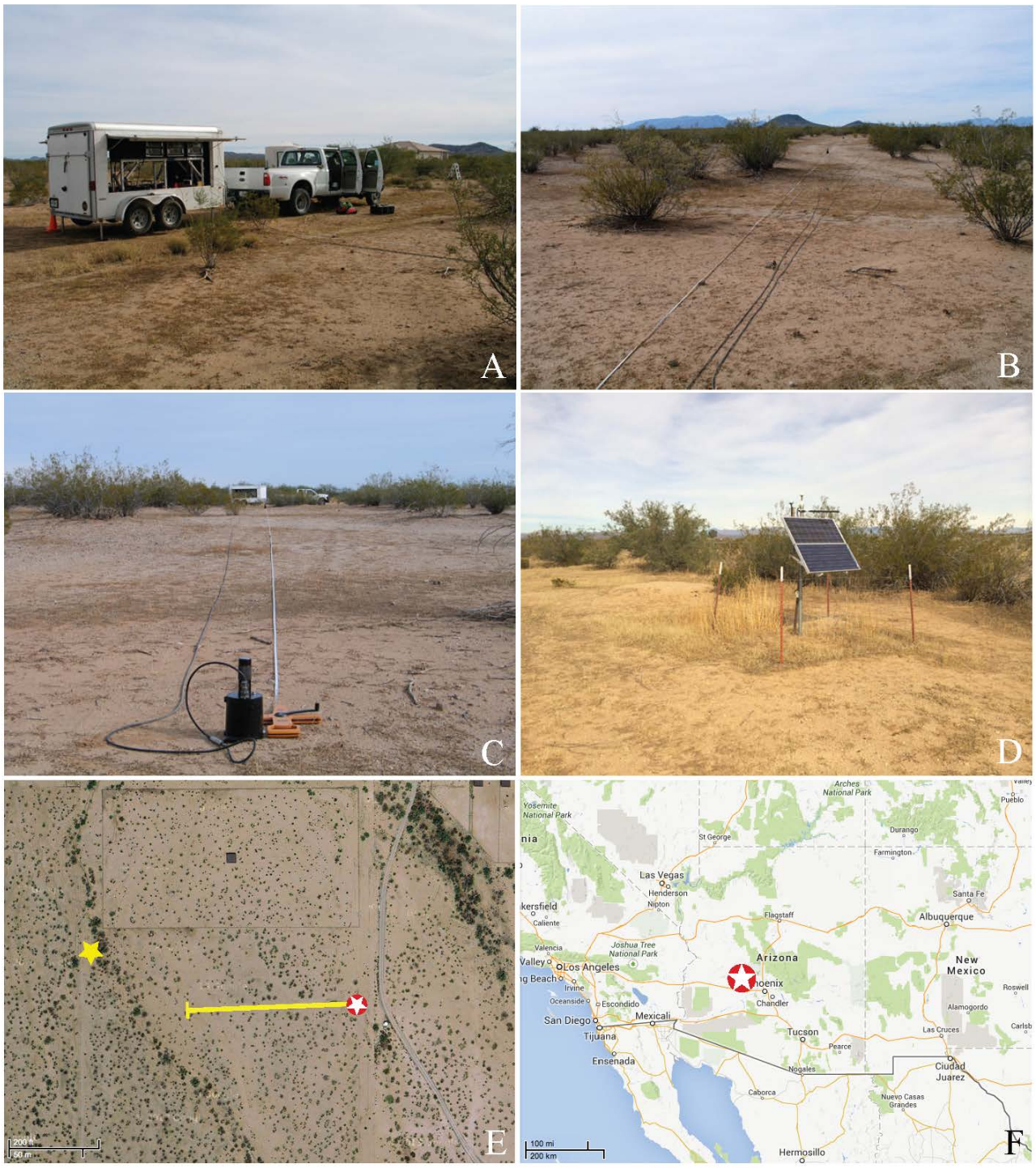

Figure 16. Surface wave test site 1001AZ-Y14A located (lat 33.93792, long –113.00282) 25 kilometers west of Wickenburg, Arizona. *A*, view to the southeast to the shaker trailer; *B*, view west to the seismometer array; *C*, view east to the shaker trailer; *D*, view northeast to the USArray seismometer location; *E*, satellite view of the local site, yellow bar is seismometer array, yellow star is the USArray seismometer location; *F*, site location in Arizona.

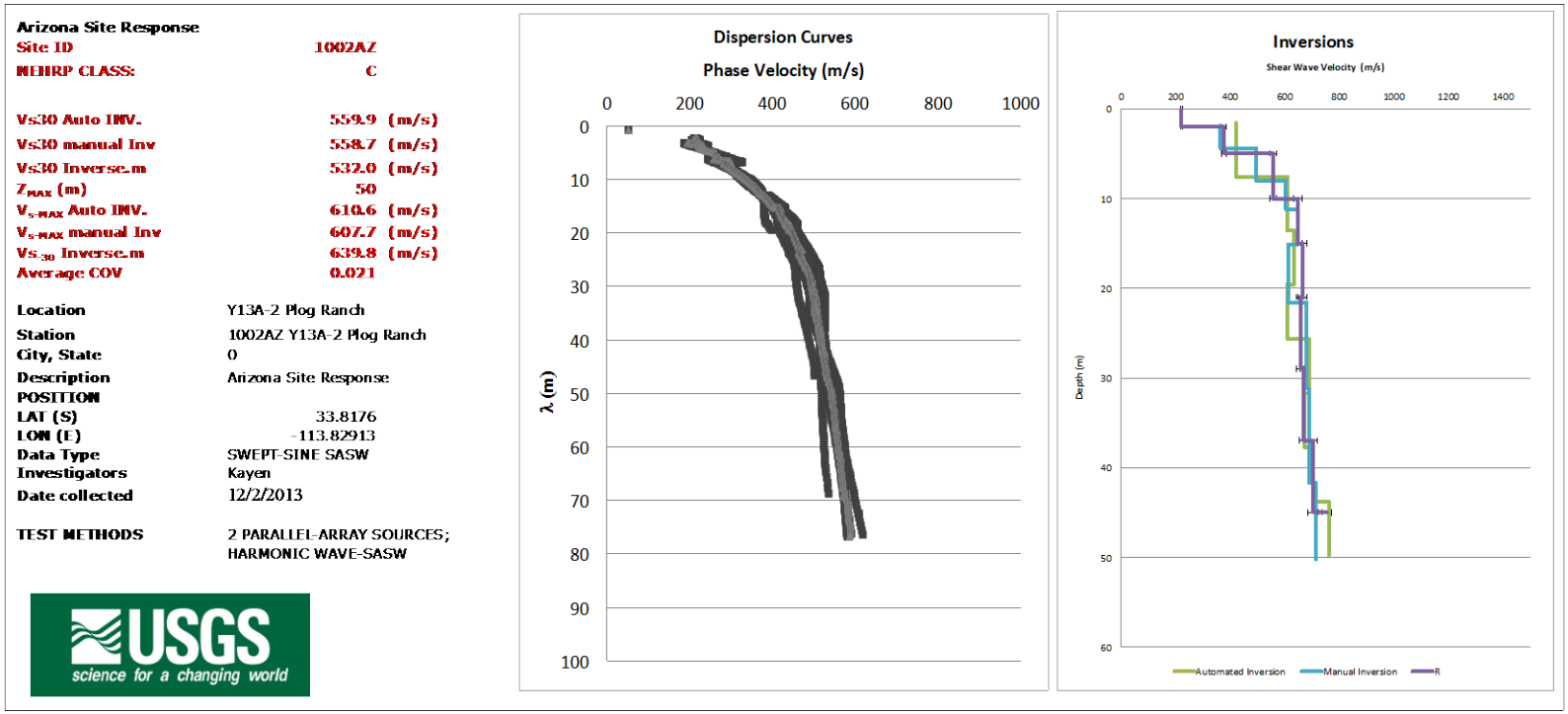

Figure 17. Site ID, location, and average shear wave velocity (left) for surface wave test site 1002AZ-Y13A-2; average dispersion curve in gray, and individual empirical dispersion curves in black (center plot); shear wave velocity profile computed by three inversion methods (right plot).

Figure 18. Surface wave test site 1002-Y13A-2 located (lat 33.8176, long –113.82913), 20 kilometers west-northwest of Salome, Arizona. *A*, view northward to the shaker trailer; *B*, view to the east to the seismometer array; *C*, view west to the shaker trailer, 100 meters from the trailer; *D*, view to the south from the shaker trailer; *E*, satellite view of the local site, yellow bar is seismometer array, the yellow star is the former location of the USArray seismometer; *F*, site location in Arizona.

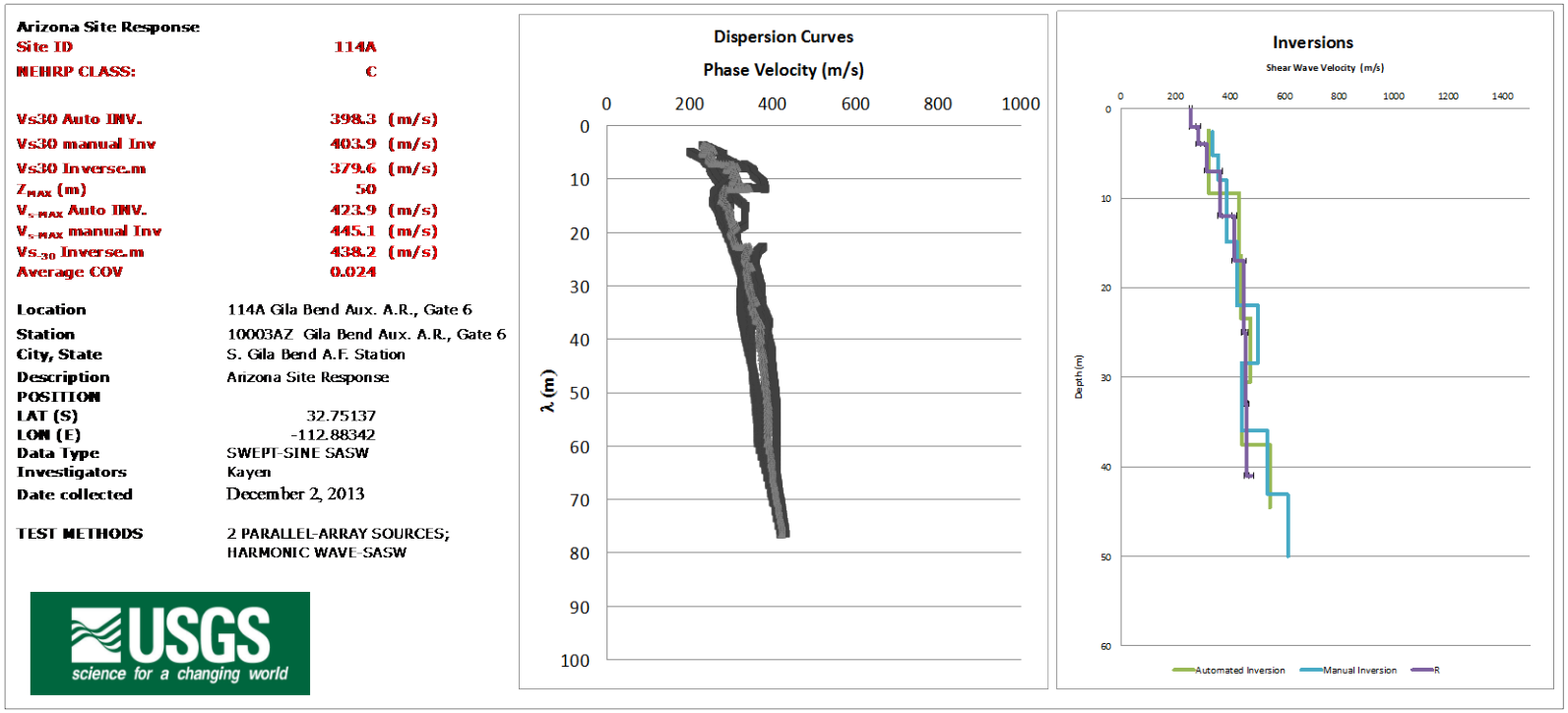

Figure 19. Site ID, location, and average shear wave velocity (left) for surface wave test site 1003AZ-114A; average dispersion curve in gray, and individual empirical dispersion curves in black (center plot); shear wave velocity profile computed by three inversion methods (right plot).

Figure 20. Surface wave test site 1003AZ-114A located (lat 32.75137, long –112.88342) on the U.S. Air Force Barry M. Goldwater Gunnery Range (BMGR East), Range 4, 26 kilometers southwest of Gila Bend, Arizona. *A*, view towards the east from the shakers to the trend of the seismometer array; *B*, view northward to the shaker trailer; *C*, view northeast across the seismometer array; *D*, another view to the north near the shaker trailer; *E*, satellite view of the local site, yellow bar is seismometer array, the yellow star is the location of the USArray seismometer; *F*, site location in Arizona.

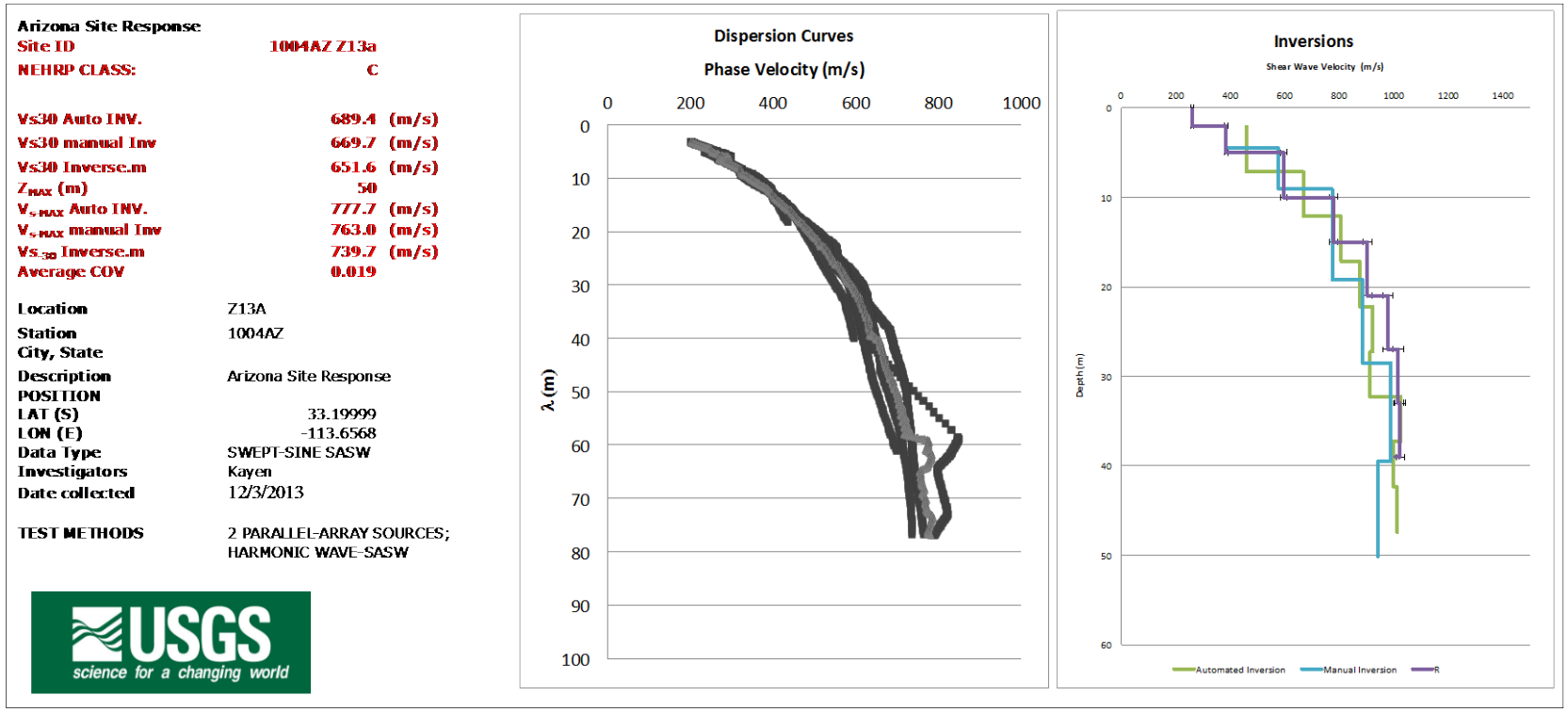

Figure 21. Site ID, location, and average shear wave velocity (left) for surface wave test site 1004AZ-Z13A; average dispersion curve in gray, and individual empirical dispersion curves in black (center plot); shear wave velocity profile computed by three inversion methods (right plot).

Figure 22. Surface wave test site 1004AZ-Z13A located (lat 33.20064, long –113.6506) 90 kilometers northwest of Gila Bend, Arizona. The test site is located about 600 meters east-northeast of the USArray seismometer location. *A*, view eastward from the shaker trailer to the seismometer array; *B*, view eastward to the shaker trailer; *C*, view northeast to the shaker trailer; *D*, view to the northwest; *E*, satellite view of the local site, yellow bar is seismometer array; *F*, site location in Arizona.

ISSN 2331-1258 (online)
https://doi.org/10.3133/ofr20161208